Characterization of the Redox Centers in Dimethyl Sulfide Dehydrogenase from *Rhodovulum sulfidophilum*†

Christopher A. McDevitt,[‡,§] Graeme R. Hanson,*[,§,||] Christopher J. Noble,[§,||] Myles R. Cheesman,[⊥] and Alastair G. McEwan*[,‡,§]

Department of Microbiology and Parasitology, School of Molecular and Microbial Sciences, Centre for Magnetic Resonance, and Centre for Metals in Biology, The University of Queensland, St. Lucia 4072, Australia, and School of Chemical Sciences, University of East Anglia, Norwich NR4 7TJ, U.K.

Received May 31, 2002; Revised Manuscript Received October 1, 2002

ABSTRACT: Dimethyl sulfide dehydrogenase from the purple phototrophic bacterium *Rhodovulum sulfidophilum* catalyzes the oxidation of dimethyl sulfide to dimethyl sulfoxide. Recent DNA sequence analysis of the *ddh* operon, encoding dimethyl sulfide dehydrogenase (*ddhABC*), and biochemical analysis (*1*) have revealed that it is a member of the DMSO reductase family of molybdenum enzymes and is closely related to respiratory nitrate reductase (NarGHI). Variable temperature X-band EPR spectra (120−122 K) of purified heterotrimeric dimethyl sulfide dehydrogenase showed resonances arising from multiple redox centers, Mo(V), $[3Fe\text{-}4S]^+$, $[4Fe\text{-}4S]^+$, and a *b*-type heme. A pH-dependent EPR study of the Mo(V) center in ^1H_2O and ^2H_2O revealed the presence of three Mo(V) species in equilibrium, Mo(V)−OH_2, Mo(V)−anion, and Mo(V)−OH. Above pH 8.2 the dominant species was Mo(V)−OH. The maximum specific activity occurred at pH 9.27. Comparison of the rhombicity and anisotropy parameters for the Mo(V) species in DMS dehydrogenase with other molybdenum enzymes of the DMSO reductase family showed that it was most similar to the low-pH nitrite spectrum of *Escherichia coli* nitrate reductase (NarGHI), consistent with previous sequence analysis of DdhA and NarG. A sequence comparison of DdhB and NarH has predicted the presence of four [Fe-S] clusters in DdhB. A $[3Fe\text{-}4S]^+$ cluster was identified in dimethyl sulfide dehydrogenase whose properties resembled those of center 2 of NarH. A $[4Fe\text{-}4S]^+$ cluster was also identified with unusual spin Hamiltonian parameters, suggesting that one of the iron atoms may have a fifth non-sulfur ligand. The *g* matrix for this cluster is very similar to that found for the minor conformation of center 1 in NarH [Guigliarelli, B., Asso, M., More, C., Augher, V., Blasco, F., Pommier, J., Giodano, G., and Bertrand, P. (1992) *Eur. J. Biochem. 307*, 63−68]. Analysis of a *ddhC* mutant showed that this gene encodes the *b*-type cytochrome in dimethyl sulfide dehydrogenase. Magnetic circular dichroism studies revealed that the axial ligands to the iron in this cytochrome are a histidine and methionine, consistent with predictions from protein sequence analysis. Redox potentiometry showed that the *b*-type cytochrome has a high midpoint redox potential ($E° = +315$ mV, pH 8).

Dimethyl sulfide dehydrogenase (DMS DH)[1] (also known as dimethyl sulfide:acceptor oxidoreductase) catalyzes the oxidation of dimethyl sulfide (DMS) to dimethyl sulfoxide (DMSO). This enzyme enables the purple photosynthetic bacterium *Rhodovulum sulfidophilum* to grow photoautotrophically with DMS as the sole electron donor (*2*). The enzyme purified from this bacterium has been shown to be a heterotrimer composed of three subunits of apparent $M_r =$ 94000 (α-subunit), 38000 (*β*-subunit), and 32000 (*γ*-subunit) (*3*). A pterin molybdenum cofactor (Moco) is present in DMS DH (*3*), and recently we showed that this prosthetic group is bis(molybdopterin guanine dinucleotide)Mo (*1*). The presence of this form of Moco is characteristic of molybdopterin- (MPT-) containing enzymes of the DMSO reductase family (*4*, *5*). Enzymes of this family have a key role in a variety of anaerobic respiratory and substrate−oxidation pathways in prokaryotes. Recently, the *ddhABDC* operon that encodes DMS DH was cloned and sequenced (*1*). As expected, the *ddhA* gene, encoding the DMS DH α-subunit, had sequence homology to genes encoding the MPT-containing subunits in enzymes of the DMSO reductase family. Protein phylogenetic analysis indicated that DMS DH was most closely related to selenate reductase, ethylbenzene dehydrogenase, and respiratory nitrate reductase (NarGHI). The comparison with nitrate reductase was particularly

† This work was partially supported by grants from the Australian Research Council to A.G.M. and G.R.H. C.A.M. thanks the University of Queensland for a postgraduate research scholarship and a graduate school travel award.

* To whom correspondence should be addressed. Tel: +61 7 3365 4878 (A.G.M.); +61 7 3365 3242 (G.R.H.). Fax: +61 7 3365 4620 (A.G.M.); +61 7 3365 3833 (G.R.H.). E-mail: mcewan@mailbox.uq.edu.au; Graeme.Hanson@cmr.uq.edu.au.

‡ Department of Microbiology and Parasitology, School of Molecular and Microbial Sciences, The University of Queensland.

§ Centre for Metals in Biology, The University of Queensland.

|| Centre for Magnetic Resonance, The University of Queensland.

⊥ School of Chemical Sciences, University of East Anglia.

[1] Abbreviations: DMS, dimethyl sulfide; DMS DH, dimethyl sulfide dehydrogenase; DMSO, dimethyl sulfoxide; MGD, molybdopterin guanine dinucleotide; Moco, molybdenum cofactor; CT, charge transfer; EPR, electron paramagnetic resonance; NIR, near-infrared; MCD, magnetic circular dichroism; *E.*, *Escherichia*; *R.*, *Rhodovulum*; cyt, cytochrome; Bicine, *N*,*N*-bis(2-hydroxyethyl)glycine; CAPS, *N*-cyclohexyl-3-aminopropanesulfonic acid; MES, 2-(4-morpholino)ethanesulfonic acid; SDS, sodium dodecyl sulfate; TEMPO, 2,2,6,6-tetramethylpiperidinyloxy; Tricine, *N*-[tris(hydroxymethyl)methyl]glycine; Tris, 2-amino-2-(hydroxymethyl)-1,3-propanediol.

10.1021/bi026221u CCC: $22.00
Published on Web 11/23/2002

informative since the molecular biology and spectroscopic properties of this enzyme have been described in detail (*6*, *7*). The NarH polypeptide of nitrate reductase contains three [4Fe-4S] iron−sulfur clusters and one [3Fe-4S] iron−sulfur cluster (*8*). Alignment of the amino acid sequences of NarH and DdhB showed that the cysteine residues involved in iron−sulfur cluster formation were conserved. This strongly suggested that the DMS DH β-subunit contained multiple iron−sulfur clusters, as seen in nitrate reductase, and this was consistent with iron analysis of DMS DH, which indicated 17 mol of Fe/mol of enzyme (*1*). This type of β-subunit is also found in closely related selenate reductase and ethylbenzene dehydrogenase as well as the more distantly related enzymes of the DMSO reductase family such as formate dehydrogenase N (*9*).

The NarGH complex of nitrate reductase is bound to the cytoplasmic face of the cytoplasmic membrane via a third subunit (NarI) (*10*). NarI is a transmembrane protein that contains two *b*-type hemes (*11*). This subunit is essential for the quinol:nitrate oxidoreductase activity of nitrate reductase; in its absence the NarGH complex is only active with redox dyes as electron donors. DMS DH, selenate reductase, and ethylbenzene dehydrogenase differ from nitrate reductase in their cellular location. They are water-soluble periplasmic enzymes and lack a transmembrane polypeptide like NarI. The optical spectrum of DMS DH and selenate reductase is dominated by a *b*-type cytochrome that contains a single heme (*1*). Amino acid sequence analysis has shown homology between the γ-subunits of DMS DH and selenate reductase, and given the assigned role of the α-subunit and β-subunit in Moco and [Fe-S] cluster binding, respectively, we have hypothesized that the γ-subunit contains the *b*-type cytochrome (*1*). Thus, the model for catalysis in DMS DH involves oxidation of the substrate at the Mo center followed by electron transfer via the [Fe-S] clusters to the *b*-type cytochrome. The *b*-type cytochrome then acts as an electron donor to cytochrome c_2, which in turn transfers electrons to the photochemical reaction center (*1*).

The redox state of the molybdenum center changes between the Mo(VI), Mo(V), and Mo(IV) states during the catalytic cycle (*12*). The Mo(V) state is paramagnetic, and enzymes of the DMSO reductase family and related families of MPT-containing enzymes (sulfite oxidase and xanthine dehydrogenase families) have been extensively studied by EPR spectroscopy (*13*−*15*). The narrow spectral line widths of Mo(V) resonances in the EPR spectra of molybdenum-containing enzymes have made it possible to identify a variety of clearly defined states. Furthermore, these individual signals define precise ligation states and coordination geometry associated with the metal (*16*). In this paper we describe the first EPR spectroscopic characterization of the Mo center of DMS DH and relate the spectra to those from other enzymes of the DMSO reductase family. Iron−sulfur clusters are also amenable to study by EPR spectroscopy, and we present herein a description of two such centers in DMS DH. Finally, we describe the spectroscopic, biochemical, and thermodynamic properties of the *b*-type cytochrome in DMS DH.

EXPERIMENTAL PROCEDURES

Growth of Bacteria, Enzyme Purification, and Assays. Growth of *R. sulfidophilum* strain SH1 and purification of DMS DH were performed as described (*1*). DMS DH activity was determined from the rate of electron transfer mediated by phenazine ethosulfate (PES) from DMS to dichlorophenolindophenol (DCPIP) under anaerobic conditions monitored at 600 nm. The assay mixture contained 1 mL of degassed 50 mM Tris-HCl, pH 8.0, plus 1 mmol of PES and 90 nmol of DCPIP. After addition of the enzyme to determine the rate of DMS-independent reduction of DCPIP, the reaction was started by addition of DMS to 20 mM from a 2 M stock solution in ethanol. DMS DH activity was calculated using ϵ_{600} for DCPIP of 21950 $M^{-1}cm^{-1}$.

Construction of a ddhC Mutant. The full-length *ddhC* gene was amplified by PCR using the forward primer DDHCLS (5′ GGATAGGAGTCTAGAATGCCCGGATTTCGG) and reverse primer DDHCSE (5′ TTCGGATGTGGTACCGTCTCAGTTCCCGG). The forward primer contained an *Xba*I restriction site while the reverse primer contained a *Kpn*I restriction site. The PCR product was cloned into the *Xba*I/*Kpn*I sites in plasmid pJP5608 (*17*). The 1.5 kb kanamycin interposon (*18*) was then cloned into the *Bam*HI site of the *ddhC* gene. The resulting construct, known as pDDHC:Km, was transformed into *Escherichia coli* strain S17-1 λpir. Plasmid pDDHC:Km was transferred to *R. sulfidophilum* by conjugation with *E. coli* strain S17 1 λpir harboring the plasmid using the filter mating method described by Masepohl et al. (*19*). Transconjugants were selected by phototrophic growth on RCV medium in the presence of 50 μg mL^{-1} Km, and double crossover mutants were then identified by sensitivity to tetracycline (10 μg mL^{-1}), indicative of loss of the suicide plasmid pJP5608.

Cell Fractionation, Western Blotting, and Heme Staining. Cells of *R. sulfidophilum* were fractionated as described by Hanlon et al. (*3*). SDS−PAGE for western blotting was performed on 10% acrylamide gels as described by Laemmli (*20*), and the separated polypeptides were transferred electrophoretically to nitrocellulose membranes (Amersham Hybond) using 10 mM CAPS−NaOH, pH 11.0, as transfer buffer. The western blot was developed using a polyclonal rabbit anti-DMS DH antibody. For the preparation of periplasmic extracts of *R. sulfidophilum* for heme-dependent peroxidase activity, proteins were partially denatured by incubation at 4 °C in standard sample buffer (*20*) in which lithium dodecyl sulfate had replaced SDS. The polypeptides in each sample were separated by SDS−PAGE at 4 °C in order to prevent loss of noncovalently bound *b*-type heme. Gels were then stained for heme-dependent peroxidase activity as described by Thomas et al. (*21*).

EPR Spectroscopy. X-band (∼9−10 GHz) continuous wave EPR spectra were recorded on either a Bruker Biospin Elexsys E500 EPR spectrometer fitted with a superhigh Q cavity or a Bruker ER200D spectrometer interfaced to an EMX control system with a dual mode (ER4116DM) X-band cavity. Calibration of the magnetic field and microwave frequency for the Elexsys E500 was achieved with a Bruker ER 035M gaussmeter and an EIP 548B microwave frequency counter, respectively. A flow-through cryostat in conjunction with a Eurotherm (B-VT-2000) variable temperature controller provided temperatures of 120−140 K at the sample position in the cavity. Lower temperatures (1.5−50 K) were obtained with either an Oxford ESR910 (Elexsys E500) or an ESR900 (EMX) flow-through cryostat in conjunction with an Oxford Instruments ITC-4 temperature controller. Spec-

trometer (Elexys E500) tuning, signal averaging, and subsequent spectral comparisons and plotting were performed with Bruker's Xepr (version 2.1) software.

Computer simulation of the EPR spectra was performed using version 1.0.4 of XSophe running on an SGI O2 R5K workstation (*22*, *23*). Simulation of the Mo(V) spectra did not attempt to reproduce the molybdenum hyperfine resonances. The computational program SOPHE employs a number of methods, including matrix diagonalization, SOPHE interpolation, and homotopy for the analysis of randomly oriented EPR spectra. In this research we employed matrix diagonalization in conjunction with mosaic misorientation to simulate the randomly oriented EPR spectra from the Mo(V) and [Fe-S] clusters. This method (C. J. Noble, K. E. Gates, and G. R. Hanson, unpublished results) significantly reduces the computational times. Comparisons of simulated and experimental spectra and data manipulation were performed with Xepr. Spin quantitation of the Mo(V) EPR resonances was performed using a double mode (TE_{104}) cavity employing TEMPO as a standard (*24*). The difference in B_1 field strengths between the two cavities was taken into account by comparing the signal intensities of the standard sample in both cavities.

MCD Spectroscopy. Electronic absorption spectra were recorded using a Hitachi U4001 spectrophotometer. MCD spectra were recorded using circular dichrographs, JASCO models J-500D and J-730 for the UV−visible and near-infrared regions, respectively. An Oxford Instruments superconducting solenoid with a 25 mm ambient temperature bore was used to generate a magnetic field of 6 T for the room temperature MCD measurements. Low-temperature MCD measurements were made using an Oxford Instruments SM4 split-coil superconducting solenoid generating a magnetic field of 5 T. Low-temperature MCD intensities ($\Delta\epsilon$) are plotted in units of M^{-1} cm^{-1} at a stated magnetic field, which in this work was 5 T. At room temperature, MCD intensities are linearly dependent on magnetic field and are plotted normalized to magnetic field as $\Delta\epsilon/H$ (M^{-1} cm^{-1} T^{-1}). To obtain optical quality glasses on freezing for low-temperature MCD measurements, glycerol was added to samples to a level of 50% v/v (*25*). That these additions had no effect on the state of the cytochrome was verified by measuring absorption and EPR spectra prior to recording the MCD spectra.

Redox Potentiometry. Mediated spectrophotometric redox potentiometry was undertaken essentially as described by Dutton (*26*). Titrations were performed in a 4 mL glass cuvette fitted with a butyl rubber bung fitted with an electrode and ports for gas entry and exit and reagent additions. Titrations were performed under an argon atmosphere at 298 K. A Pt−Ag/AgCl combination microelectrode (Kent-Taylor) was calibrated with a saturated solution of quinhydrone (hydroquinone/benzoquinone 1:1 complex; $E_0' = +295$ mV) for 1 h prior to the titration. Redox active dyes were used as redox mediators during the titration at a final concentration of 10 μM. The selection of redox dyes spanning the range of the titration was as follows: diaminodurine, +250 mV; 2,6-dimethylbenzoquinone, +180 mV; phenazine methosulfate, +80 mV; phenazine ethosulfate, +55 mV; menaquinone, −30 mV. The ambient redox potential of the system was controlled by using aliquots of reductant (sodium dithionite) or oxidant (potassium ferricyanide). After the addition of reductant or oxidant the system was allowed 10 min to come to equilibrium (at which point the measured potential remained steady) before an absorption spectrum of the sample was measured between 500 and 700 nm. The absorbance at the α-max wavelength (569 nm) for the reduced cytochrome minus the absorbance at the isobestic point (560 nm) was measured as a function of redox potential. These data were fitted to the Nernst equation using Tablecurve (Jandel Scientific) and Sigmaplot (SPSS).

RESULTS

EPR Studies of the Mo Center in DMS DH. Variable temperature X-band EPR spectra of resting DMS DH at 120 K (Figures S1 and 2a) consisted of three dominant resonances, each flanked by six weaker resonances. The relative intensities of these resonances are consistent with naturally abundant molybdenum, which consists of a mixture of isotopes (^{92,94,96,98,100}Mo, 75%, $I = 0$; ^{95,97}Mo, 25%, $I = {}^5/_2$). The g anisotropy, narrow line widths (0.9−1.1 mT), and temperature dependence of the resonances are consistent with a Mo(V) center containing a single unpaired electron, d^1 ($S = {}^1/_2$). Spin quantitation (*24*) revealed that 28% of the Mo found in resting DMS DH is present as Mo(V).

Closer examination of the $I = 0$ resonances as a function of pH (Figure 1a, pH 6.0, and Figure 1b, pH 8.2) revealed shoulders (labeled with a vertical bar and an asterisk) on the three resonances, which may arise from multiple species and/or proton hyperfine coupling. Increasing the pH from 6.0 to 8.2 enhanced the intensity of the shoulders labeled with a vertical bar, suggesting the presence of multiple species. The EPR spectrum of DMS DH in ^2H_2O (Figure 1e) shows that the line shape of the $g = 1.9600$ and $g = 1.9989$ resonances remained unchanged, confirming the presence of at least two species. In contrast, the shoulder labeled with an asterisk completely disappeared upon deuteration, indicating that this shoulder must arise from proton hyperfine coupling. The reduction in line width arising from the smaller value of $g_n\beta_n$ for deuterium (0.857440 μB) versus hydrogen (2.79285 μB) enabled the resolution of the third resonance ($g = 1.9805$) associated with the species, giving rise to the resonances labeled with a vertical bar. Computer simulation of these resonances with an orthorhombic electron Zeeman spin Hamiltonian (eq 1, term 1) and the g matrix (for the species Mo−X) listed in Table 1 yielded the spectrum shown in Figure 1d.

$$H = \beta \underline{B} \underline{g} \underline{S} + \sum_{i=1,2} (\underline{S} \underline{A}_i \underline{I}_i - g_n \beta_n \underline{B} \underline{I}_i) \qquad (1)$$

As previously mentioned, the central resonance ($g = 1.9846$) associated with the major species exhibits proton hyperfine coupling. Since there was no shift in the resonant field position upon deuteration, there must be an even number of protons giving rise to the resonance labeled with an asterisk. The simplest situation is two magnetically equivalent protons that lead to three resonances with the intensity distribution 1:2:1. Computer simulation of the resonances associated with the major species with an orthorhombic spin Hamiltonian (eq 1) and the g and A matrixes (for the species Mo−OH_2) listed in Table 1 yields the spectrum shown in Figure 1c. Changing the proportions of the ^{1}H ($I = {}^1/_2$, 99.985%) and ^{2}H ($I = 1$, 0.015%) isotopes to 0.01% and

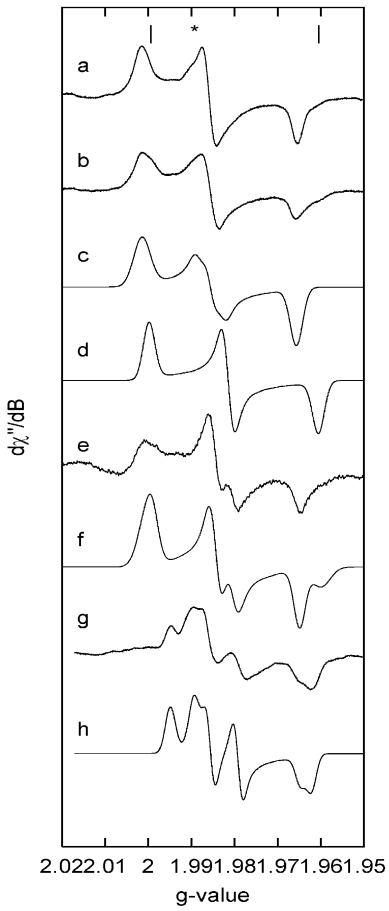

FIGURE 1: X-band EPR spectra of DMS DH (1.0 mg/mL) as a function of pH at 120 K. (a) pH 6.0, 50 mM MES−NaOH and ^1H_2O buffer. (b) pH 8.2, 50 mM Bicine−NaOH and ^1H_2O buffer. (c, d) Computer simulation of the EPR spectra from the two components (Mo−OH_2 and Mo−X) present in the EPR spectrum shown in (b). Spin Hamiltonian parameters are given in Table 1. (e) pH 8.2, 1.0 mg/mL in 50 mM Bicine−NaOH and ^2H_2O buffer. The broad resonance around $g = 2.01-2.02$ arises from adventitious copper(II). (f) Computer simulation of the EPR spectrum shown in (e) by adding the simulated spectra in ^2H_2O from Mo−OH_2 (62.5%) and Mo−X (37.5%). (g) pH 11.0, 100 mM CAPS−NaOH and ^1H_2O buffer. (h) Computer simulation of the EPR spectrum shown in (g). Spin Hamiltonian parameters are given in Table 1.

99.99%, respectively, in XSophe reproduced the line shape of the $g = 1.9846$ resonance in the deuterated spectrum (Figure 1e) (results not shown). Addition of this spectrum and Figure 1d in the ratio 0.625:0.375 produced the spectrum shown in Figure 1f that reproduces the experimental spectrum shown in Figure 1e.

Increasing the pH to 11.0 yielded the EPR spectrum of DMS DH shown in Figure 1g. Clearly, there is hyperfine coupling from a single proton. Computer simulation of this spectrum assuming an orthorhombic spin Hamiltonian and the *g* and *A* matrices (for Mo−OH) listed in Table 1 yielded the spectrum shown in Figure 1h. The EPR results presented above are consistent with the equilibria:

$$\text{Mo}-\text{OH}_2 + \text{X}^- \leftrightarrow \text{Mo}-\text{X} + \text{H}_2\text{O}$$

and

$$\text{Mo}-\text{OH}_2 + \text{OH}^- \leftrightarrow \text{Mo}-\text{OH} + \text{H}_2\text{O} \qquad (2)$$

where X^- is probably an anion, chloride. Anion binding to Mo(V) centers in metalloenzymes has been observed for nitrate reductase (NarGHI) (*27*) and xanthine oxidase (*28*). Comparison of rhombicity and anisotropy parameters of the Mo(V) signals arising from DMS DH with those from other enzymes of the DMSO reductase family (Table 1) showed that all three signal-giving species (Mo−X, Mo−OH, and Mo−OH_2) were more similar to the low-pH nitrite spectrum of nitrate reductase (NarGH) from *E. coli* than other enzymes of the DMSO reductase family (*29*).

EPR Spectroscopy of the [Fe-S] Clusters and b-Type Heme in DMS DH. At 120 K the EPR spectrum of DMS DH is dominated by three resonances whose *g* anisotropy, narrow line widths (0.9−1.1 mT), and temperature dependence are consistent with a Mo(V) signal-giving species. Decreasing the temperature from 120 to 2 K (Figure 2a−c) results in the appearance of resonances, additional to those derived from the Mo(V) center, that must arise from one or more species with fast spin−lattice relaxation times, T_1. At 5 K the EPR spectrum (Figure 2b) around $g = 2$ consisted of resonances arising from the Mo(V) center with overlapping resonances that are characteristic of those arising from [3Fe-4S]$^{1+}$ clusters (*30*). An EPR spectrum recorded over a field range 0−1.5 T revealed additional resonances ($g_{\text{eff}} = 4.3$ and 0.5) from high-spin Fe(III), probably adventitious Fe(III). At lower temperatures (2 K) the resonances from the Mo(V) center become saturated, and the EPR spectrum (Figure 2c) was almost entirely associated with the [3Fe-4S]$^{1+}$ cluster. Computer simulation of this spectrum with an orthorhombic spin Hamiltonian (eq 1, term 1) and the *g* matrix listed in Table 2 yields the spectrum shown in Figure 2d. Addition of the spectrum in Figure 2a and the spectrum in Figure 2d yielded the spectrum shown in Figure 2c (results not shown), confirming that if the Mo(V) and the [3Fe-4S]$^+$ cluster are interacting, then the dipole−dipole interaction must be very small; i.e., the distance between the two centers is large.

A close examination of the low-temperature spectra (Figure 2b,c) revealed weak resonances around 360−370 mT. Increasing the temperature to 25 K produced the EPR spectrum shown in Figure 2e. At this temperature the [3Fe-4S]$^{1+}$ cluster is relaxing too fast to be detected, and the EPR spectrum consisted of resonances from the Mo(V) center and an additional putative [4Fe-4S]$^+$ cluster. Computer simulation of these resonances with the rhombic *g* matrix given in Table 3 and a rhombic spin Hamiltonian (eq 1, term 1) produced the spectrum in Figure 2f. The intensity of these resonances was found to increase upon reduction of DMS dehydrogenase with sodium dithionite and decrease upon oxidation with ferricyanide (results not shown). The spin Hamiltonian parameters (Table 3) indicate that the [4Fe-4S]$^+$ center associated with DMS dehydrogenase are different to those of the major conformation of center 1 in NarH and DmsB center 1 (*31, 32*) but were very similar to the minor conformation of center 1 in NarH that has been reported previously (*33*).

Oxidation of DMS DH with ferricyanide resulted in a decrease in the signal intensity of the resonances of the [4Fe-4S]$^+$ cluster and the Mo(V) center. In contrast, the resonances from the [3Fe-4S]$^+$ cluster were found to increase, and a new resonance was observed at $g_1 = 3.34$ (Figure 3) which can be attributed to a low-spin ferric heme [Fe(III), $S = {}^1/_2$].

Table 1: Spin Hamiltonian Parameters for the Mo(V) Species in DMS Dehydrogenase and Related Enzymes of the DMSO Reductase Family of Molybdoenzymes[a]

sample	enzyme type	center	g_1	g_2	g_3	g_{av}	anisotropy	rhombicity	ref
DMS DH[b]	II	Mo(V)−aqua	1.9650	1.9846	2.0006	1.9834	0.0356	0.45	this work
DMS DH[c]	II	Mo(V)−X	1.9600	1.9805	1.9989	1.9798	0.0389	0.47	this work
DMS DH[d]	II	Mo(V)−OH	1.9627	1.98	1.9914	1.9785	0.0287	0.40	this work
NarGHI[i]	II	Mo(V) low pH nitrite type 1	1.9642	1.9851	1.9997	1.9830	0.0355	0.41	*29*, *56*
DmsABC[j]	II	Mo(V)	1.960	1.980	1.984	1.9746	0.0240	0.167	*57*
DMSOR[e]	III	Mo(V) high *g* unsplit	1.9611	1.9833	1.9906	1.9783	0.0238	0.16	*42*
DMSOR[e,f]	III	Mo(V) high *g* split	1.9673	1.9818	1.9922	1.9804	0.0249	0.42	*42*
FDH[g]	I	Mo(V)	1.9630	1.9880	2.0190	1.9900	0.0560	0.55	*58*
NAP[h]	I	Mo(V) high *g* resting	1.9806	1.9902	1.9985	1.9898	0.0194	0.51	*43*

[a] Parameters used for dehydrogenase are those used for the computer simulations in Figure 1. Anisotropy ($g_3 - g_1$) and rhombicity [$(g_3 - g_2)/(g_3 - g_1)$] parameters are provided to allow comparisons between signals. [b] DMS DH: dimethyl sulfide dehydrogenase. Mo(V)−aqua: two equivalent protons, A_2 (^{1}H) = 4.0×10^{-4} cm^{-1}. [c] X may represent an anion, such as chloride. [d] Mo(V)−OH: A_1 (^{1}H) = 8.9×10^{-4} cm^{-1}, A_2 (^{1}H) = 10.5×10^{-4} cm^{-1}, and A_3 (^{1}H) = 4.1×10^{-4} cm^{-1}. [e] DMSOR: dimethyl sulfoxide reductase from *Rhodobacter capsulatus*. [f] DMSOR: *R. capsulatus*. Mo(V) high *g* split: A_1 (^{1}H) = 1.056×10^{-4} cm^{-1}, A_2 (^{1}H) = 0.971×10^{-4} cm^{-1}, and A_3 (^{1}H) = 1.349×10^{-4} cm^{-1}. [g] FDH: formate dehydrogenase from *Desulfovibrio desulfuricans* ATCC 27774. [h] NAP: periplasmic nitrate reductase from *Paracoccus denitrificans*. Mo(V) high *g* resting: A_1 (^{1}H) = 4.7×10^{-4} cm^{-1}, A_2 (^{1}H) = 4.7×10^{-4} cm^{-1}, and A_3 (^{1}H) = 6.0 and 2.8×10^{-4} cm^{-1}. [i] NarGHI: nitrate reductase from *E. coli*. Mo(V) low pH nitrite: A_1 (^{1}H) = 0.954×10^{-4} cm^{-1}, A_2 (^{1}H) = 0.964×10^{-4} cm^{-1}, and A_3 (^{1}H) = 1.466×10^{-4} cm^{-1}. [j] DmsABC: *E. coli* DMSO reductase. Mo(V) resting spectrum at 75 K.

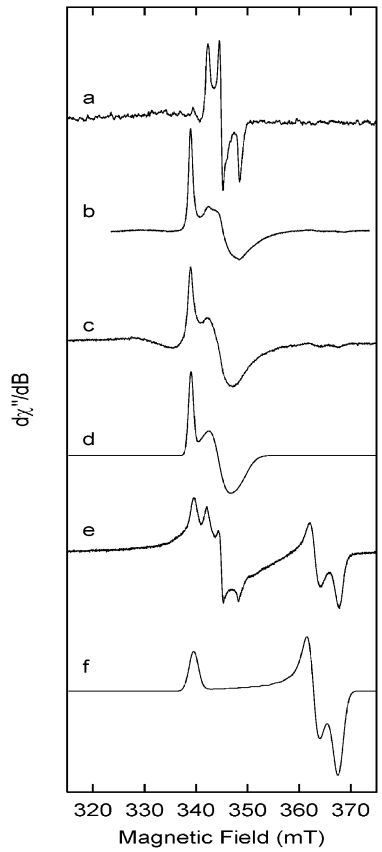

FIGURE 2: Variable temperature X-band (ν = 9.4667 GHz) EPR spectra of DMS DH (1.0 mg/mL in 50 mM Tris-HCl, pH 8.0). (a) T = 120 K. (b) T = 5 K. (c) T = 2 K. (d) Computer simulation of the EPR spectrum from the [3Fe-4S]$^{1+}$ cluster shown in (c). Spin Hamiltonian parameters are given in Table 2. (e) T = 25 K. (f) Computer simulation of the EPR spectrum from the [4Fe-4S]$^{+}$ cluster shown in (e). Spin Hamiltonian parameters are given in Table 3.

The g_2 and g_3 resonances are either hidden underneath those from the [3Fe-4S]$^{+}$ cluster or are too broad to be observed (i.e., the spin−lattice relaxation times are highly anisotropic and very short). High-field EPR measurements should enable the determination of the complete *g* matrix for the low-spin ferric heme.

Table 2: Spin Hamiltonian Parameters for the [3Fe-4S]$^{1+}$ Clusters in DMS Dehydrogenase and Related Species from Other Enzymes

sample	center	g_1	g_2	g_3	g_{av}	ref
DMS DH	[3Fe-4S]$^{1+}$	1.9650	1.9870	2.0180	1.9900	this work
NAR[a] center 2	[3Fe-4S]$^{1+}$			2.0		*31*
GDfd[b]	[3Fe-4S]$^{1+}$	1.9500	1.9799	2.0210	1.9836	*59*

[a] NAR: membrane-bound respiratory nitrate reductase purified from *E. coli*. [b] GDfd: ferredoxin purified from *Giardia duodenalis*.

Identification of ddhC as the Location of the b-Type Cytochrome in DMS DH. A strain of *R. sulfidophilum* deficient in *ddhC* was generated as described in the Experimental Procedures, and its genotype was confirmed via PCR analysis. Photoheterotrophic growth of the *ddhC* mutant was unaffected, but it was unable to grow photoautotrophically with DMS as sole electron donor (data not shown). However, it was possible to assess the state of DMS DH in the *ddhC* mutant because photoheterotrophic growth of *R. sulfidophilum* in the presence of DMS induces the enzyme (*2*, *3*). Periplasmic fractions were obtained from such cells, and activity assays indicated that in both the mutant and the wild-type strains the PES-dependent DMS:DCPIP oxidoreductase activity levels were similar. Western blot analyses, employing an anti-DMS DH antibody (*1*), showed that the DMS DH produced in the *ddhC* mutant strain lacked the 32 kDa subunit (Figure 4a) but contained the higher molecular mass subunits DdhA and DdhB. This confirmed that the remaining components of the DMS DH enzyme were expressed in the *ddhC* mutant. Heme-dependent peroxidase staining of an SDS−PAGE gel of the periplasmic fractions from the wild-type strain and *ddhC* mutant grown photoheterotrophically revealed multiple *b*- and *c*-type cytochromes that were common to both strains. However, in the 32 kDa region (Figure 4b) a heme-staining band was present in the periplasmic extracts of wild-type cells (lane 1) but was absent in the periplasmic extracts of the mutant strain (lane 2). Taken together, the data in Figure 4a strongly suggest that DdhC is the *b*-type cytochrome subunit of DMS DH.

Table 3: Spin Hamiltonian Parameters for the [4Fe-4S]$^{+}$ Clusters in DMS Dehydrogenase and Related Species from Other Enzymes and Model Compounds[a]

sample	center	g_1	g_2	g_3	g_{av}	Δg	rhombicity	ref
DMS DH center 1	[4Fe-4S]$^{+}$	1.8620	1.8870	2.0158	1.9216	0.081	0.83745	this work
NARGH[b] center 1 (major conformation)	[4Fe-4S]$^{+}$	1.87	1.9470	2.0490	1.9550	0.047	0.56667	*33*
NARGH[b] center 1 (minor conformation)	[4Fe-4S]$^{+}$	1.8710	1.8850	2.0100	1.9220	0.080	0.89928	*33*
DMSOR center 1	[4Fe-4S]$^{+}$	1.8660	1.9300	2.0100	1.9353	0.067	0.55556	*32*
FDH[c]	[4Fe-4S]$^{+}$	1.9540	1.9260	2.0710	1.9837	0.019	1.24	*58*
FDH[c]	[4Fe-4S]$^{+}$	1.8650	1.9260	2.0710	1.9540	0.048	0.70388	*58*
NAP[d]	[4Fe-4S]$^{+}$	1.8900	1.9400	2.03	1.9500	0.052	0.64285	*60*
aconitase	[4Fe-4S]$^{+}$	1.86	1.93	2.06	1.95	0.052	0.65000	*61*, *62*
aconitase/isocitrate	[4Fe-4S]$^{+}$	1.78	1.85	2.04	1.8900	0.112	0.73076	*61*, *62*
aconitase/*trans*-aconitase	[4Fe-4S]$^{+}$	1.8	1.88	2.01	1.8970	0.105	0.61940	*61*, *62*
aconitase/nitroisocitrate	[4Fe-4S]$^{+}$	1.77	1.87	2.04	1.8930	0.109	0.62962	*61*, *62*
$[Fe_4S_4(SC_6H_4\text{-}o\text{-}OH)_4]^{2+}$ (site 1)	[4Fe-4S]$^{+}$	1.979	2.028	2.138	2.048	−0.046	0.69182	*49*
$[Fe_4S_4(SC_6H_4\text{-}o\text{-}OH)_4]^{2+}$ (site 7)	[4Fe-4S]$^{+}$	1.884	1.888	2.045	1.940	0.062	0.97516	*49*
D. africanus conformation 1	[4Fe-4S]$^{+}$	1.9020	1.9500	2.0690	1.9737	0.029	0.71258	*50*
D. africanus conformation 2	[4Fe-4S]$^{+}$	1.8820	1.9410	2.0570	1.9600	0.042	0.66286	*50*
PFfd[e]	[4Fe-4S]$^{+}$ ($S = {}^1/_2$)	1.80	1.87	2.10	1.92	0.082	0.76667	*63*, *64*

[a] Δg ($g_e - g_{av}$) and rhombicity [$(g_3 - g_2)/(g_3 - g_1)$] parameters are provided to allow comparisons between signals. [b] NAR: membrane-bound respiratory nitrate reductase purified from *E. coli*. [c] FDH: formate dehydrogenase from *D. desulfuricans* ATCC 27774. [d] NAP: periplasmic nitrate reductase *Paracoccus pantotropha*. [e] PFfd: *Pyrococcus furiosus* ferredoxin. The [4Fe-4S]$^{+}$ in the wild-type protein exists as a mixture of $S = {}^1/_2$ and $S = {}^3/_2$ spin states. For the latter state $g = 1.98$, $E/D = 0.22$, and D was estimated to be 3.3 cm^{-1}.

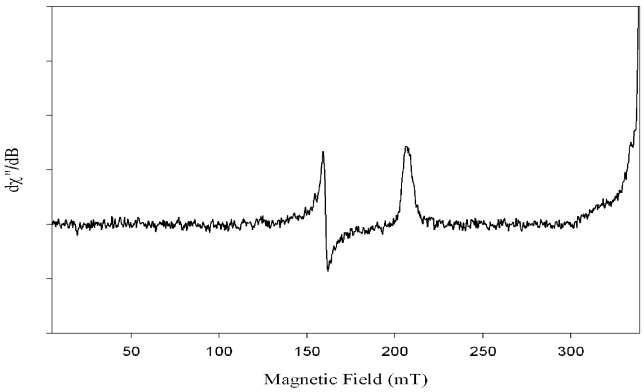

FIGURE 3: EPR spectrum of oxidized DMS dehydrogenase revealing the $g = 3.34$ resonance from the low-spin Fe(III) type *b* heme. Conditions: temperature, 10 K; microwave power, 2 mW; modulation amplitude, 1 mT; microwave frequency, 9.663 GHz.

MCD Studies of the b-Type Cytochrome: Identification of the Axial Ligands to the Low-Spin Ferric Heme. The optical and MCD spectra of a heme group varies depending on the nature of the porphyrin ring, the oxidation state of the iron, and the nature of the axial ligands to the iron (*34*). Sequence analysis of the DdhC subunit and its nearest relative, the SerC polypeptide of selenate reductase, identified two conserved amino acids (His81 and Met147 in DdhC) that might be the axial ligands to the iron.

Although DMS DH contains multiple iron−sulfur clusters, the MCD spectra of these clusters in any oxidation state are an order of magnitude less intense than that of a heme group (*25*, *34*). The UV−visible absorption (Figure 5a) and MCD spectra of ferricyanide-oxidized DMS DH at room temperature (Figure S2) and at 4.2 K (Figure 5b) showed typical low-spin ferric heme spectra. No bands characteristic of reduced ferrous hemes were observed in the absorption and MCD spectra. In addition, there was no obvious indications of high-spin ferric heme, consistent with the absence of any $g \sim 6$ features in the EPR spectrum (Figure 3).

The MCD intensities of the Soret band (428 nm) (136 M^{-1} cm^{-1} T^{-1} peak to trough at room temperature and 33 M^{-1}

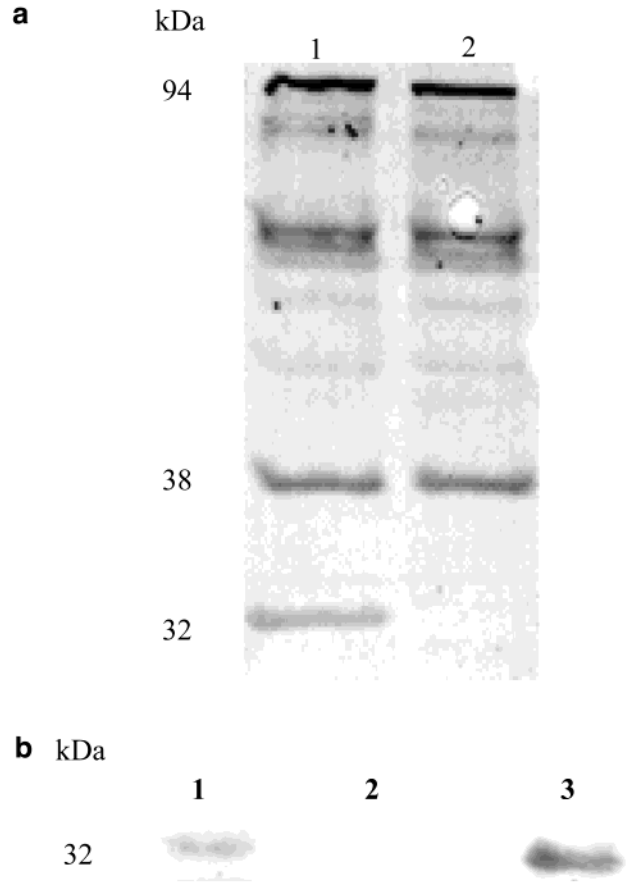

FIGURE 4: (a) Western blot of periplasmic extracts of *R. sulfidophilum* grown photoheterotrophically in the presence of 30 mM DMS. Lanes: 1, 5 μg of periplasmic extracts of the *R. sulfidophilum* wild-type strain; 2, 5 μg of periplasmic extracts of the *R. sulfidophilum ddhC*-deficient strain. (b) Heme-dependent peroxidase stain of periplasmic extracts of *R. sulfidophilum*. Lanes: 1, 5 μg of the wild-type strain grown photoheterotrophically in the presence of 30 mM DMS; 2, 5 μg of the *R. sulfidophilum ddhC*-deficient strain grown photoheterotrophically with DMS as an electron donor; 3, 5 μg of the wild-type strain grown photoheterotrophically with DMS as an electron donor.

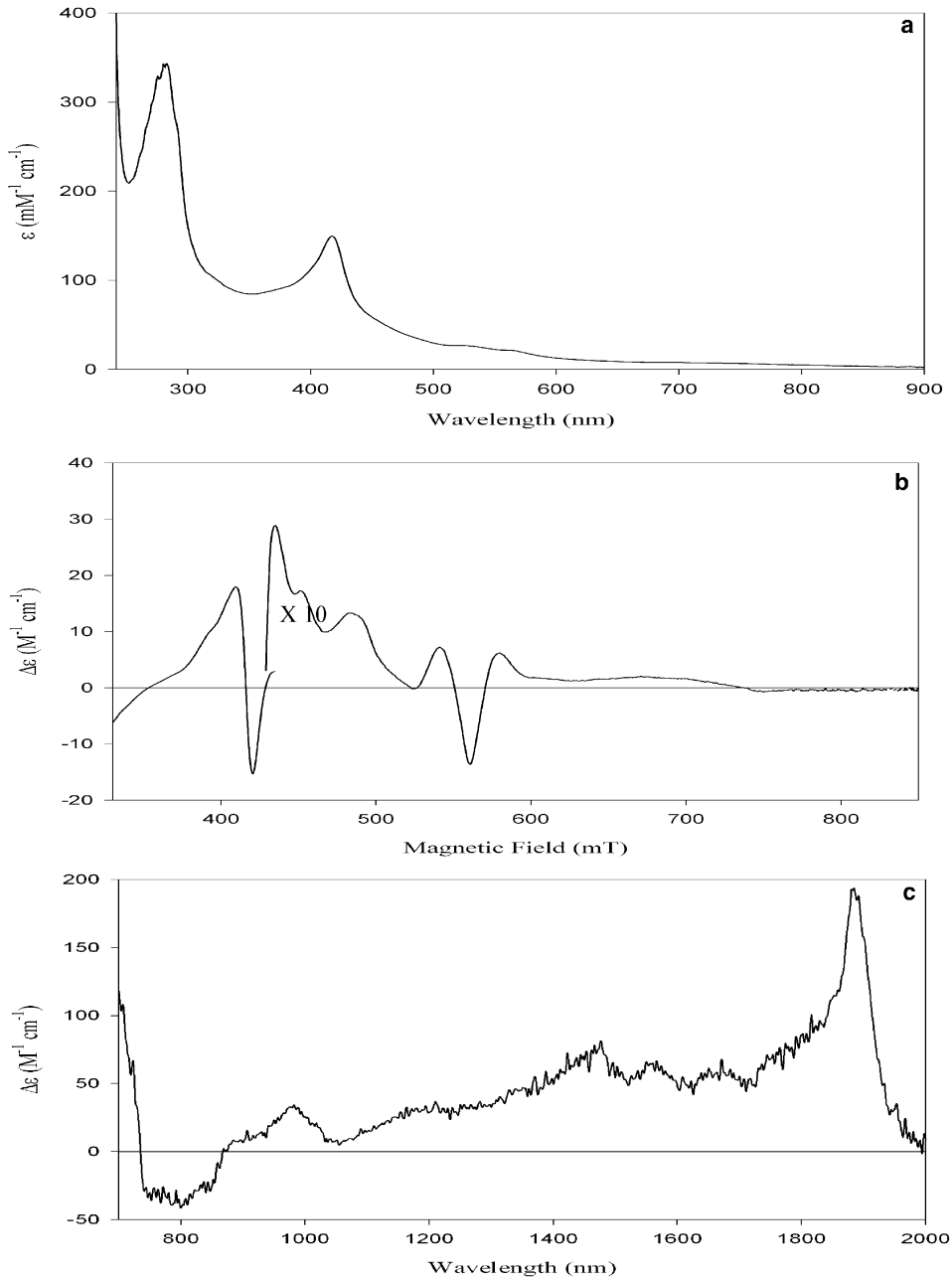

FIGURE 5: Optical and MCD spectra of oxidized DMS DH in 50 mM Tricine, pH 8.0. (a) Room temperature electronic absorption spectrum: DMS DH concentration, 82 μM. (b) MCD spectrum: DMS DH concentration, 50 μM (50% glycerol); temperature, 4.2 K; magnetic field, 5 T. (c) Near-infrared MCD spectrum: DMS DH concentration, 50 μM (50% glycerol); temperature, 4.2 K; magnetic field, 5 T.

cm^{-1} at 4.2 K) and the band in the α,β region indicate one low-spin ferric heme, obviously that giving rise to the $g = 3.34$ resonance in the EPR spectrum. The agreement between the number of hemes indicated by the absorption (*3*), MCD, and EPR eliminates the possibility of an EPR-silent spin-coupled heme which would have been observable by electronic absorption and MCD spectroscopy. The MCD spectrum (Figure 5b) reveals a weak broad band in the 600−750 nm region which is not part of a basic low-spin ferric heme spectrum and is not obvious in the absorption spectrum (Figure 5a). There are probably two contributions to this intensity: absorption bands typical for $[3Fe\text{-}4S]^{1+}$ clusters and weak charge-transfer (CT) transitions which are observed for low-spin ferric hemes with sulfur ligands (*25*, *35*−*39*).

The near-infrared (NIR) spectral region (1000−3000 nm) contains additional electronic CT transitions which are readily located using MCD spectroscopy against a background of vibrational overtone absorptions (*34*). Low-spin ferric hemes give rise to a characteristic positive porphyrin (π) to ferric (d) CT band with vibrational side structure to higher energy (*34*). The peak wavelength of this NIR-CT band is diagnostic of the heme axial ligands. For oxidized DMS DH, this band is observed at 1885 nm (Figure 5c), a wavelength which shows unambiguously that the ferric heme is axially ligated by histidine and methionine.

Thermodynamic Characterization of the b-Type Heme. As described earlier (*3*) the optical spectrum of DMS DH (Figure 5a) is dominated by a single *b*-type heme which is reduced

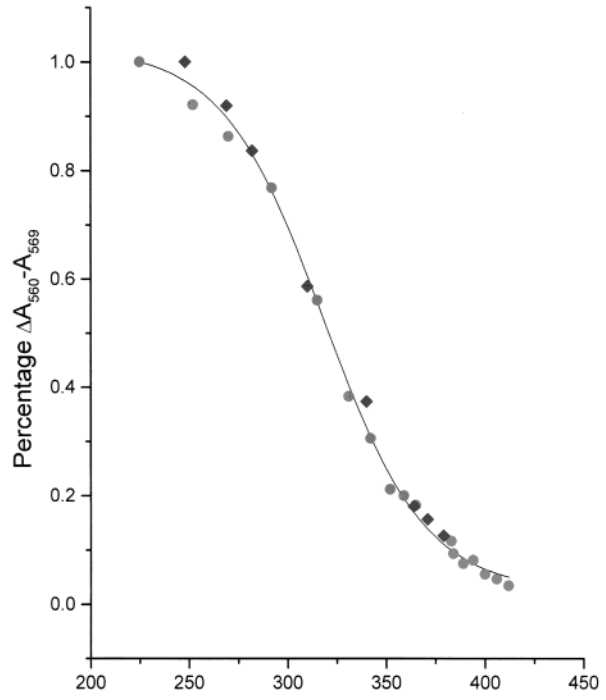

FIGURE 6: Redox potentiometric titration curve of the *b*-type cytochrome in purified DMS dehydrogenase. The absorbance changes at 560−569 nm were plotted against redox potential for both dithionite (●) and ferricyanide (◆) titrations. Theoretical curves were generated by nonlinear regression using the Nernst equation for one heme undergoing a one-electron reduction (●) or oxidation (◆).

in the resting enzyme. Consequently, it was possible to use redox potentiometry to determine the midpoint potential of the *b*-type heme by following changes in the visible absorption spectrum of this heme. Visible absorption spectra were recorded under anaerobic conditions at a variety of redox potentials (data not shown). Both the shape and the wavelength maxima of the $\alpha\beta$ bands (560 and 533 nm, respectively) were not observed to change significantly as a function of the ambient redox potential. Experimental data were fitted using nonlinear regression analysis and the Nernst equation with numerous parameters, including values of n (number of electrons) between 1 and 2 and numbers of heme species between 1 and 3. The best fit ($r^2 = 0.965$) assumes a single heme and $n = 1$ (Figure 6). The midpoint redox potential (pH 8.0) of the *b*-type heme was calculated as 315 ± 20 mV (mean ± standard deviation of three independent redox titrations).

DISCUSSION

The DMSO reductase family contains the majority of microbial molybdenum enzymes that have been characterized, and most of these enzymes are components of a respiratory chain. The identification of bis(MGD)Mo in DMS DH confirmed that this enzyme is a member of the DMSO reductase family while further sequence analysis indicated that it is related to respiratory nitrate reductase (NarGHI) (*1*). The crystal structures of enzymes of the DMSO reductase family that have emerged over the last 5 years or so show that the domain organization and tertiary structure of the MPT-containing subunit are highly conserved (*1*, *40*, *41*). Recently, we analyzed the phylogeny of enzymes within the DMSO reductase family, and our results showed that this family could be divided into three distinct clades (*1*, *5*). The enzymes (types I, II, and III) associated with the three clades have differences in the structure of the Mo active site. In type I enzymes (exemplified by periplasmic nitrate reductase and formate dehydrogenases) the Mo is ligated by a cysteine or selenocysteine amino acid side chain while in type III enzymes (exemplified by *Rhodobacter* DMSO reductase) the amino acid ligand is provided by a serine residue.

This distinction between the structure of the Mo active sites extends to the *g*-value parameters of the Mo(V) species of the signal-giving species for type I, type II, and type III enzymes (Table 1 and refs *42* and *43*). Our phylogenetic analysis places DMS DH in the type II clade, alongside nitrate reductase (NarG), selenate reductase, and ethylbenzene dehydrogenase (*1*). Hence, it was expected that the Mo(V) EPR-active species of DMS DH might be similar to those of other type II enzymes. Our observation that the *g* matrix, anisotropy, and rhombicity parameters of DMS DH and nitrate reductase are more similar than other Mo enzymes of the DMSO reductase family (Table 1) is consistent with the view that these two enzymes, and by inference the phylogenetically related enzymes selenate reductase and ethylbenzene dehydrogenase, have a similar Mo active site. In view of the similarity between the Mo(V) signal-giving species of nitrate reductase and DMS DH, it seems likely that the Mo will be ligated by the same type of amino acid side chain. Our recent sequence analysis suggests that this could be Ser195, Thr214, or His220 in DMS DH and the comparable residues in nitrate reductase (*1*).

The EPR spectroscopic study of DMS DH took advantage of the very high Mo(V) content (28%) in the resting enzyme. This is unusual for Mo enzymes, especially reductases, where the purified enzyme is usually present in the diamagnetic Mo(VI) state. The high proportion of Mo(V) in DMS DH may arise from the reoxidation of the Mo(IV) center (formed by DMS reduction of the Mo center) by single electron-transfer reactions. It would be expected that one electron would be transferred to the *b*-type cytochrome of the enzyme yielding a Mo(V) species and a ferrocytochrome *b*. Further oxidation of the Mo(V) center could only occur after the oxidation of the ferrocytochrome *b* by the cytochrome c_2 protein that has been demonstrated genetically to be the electron acceptor for DMS DH (*1*). Thus, a Mo(V) species of DMS DH may be formed during catalysis, but this form may be stabilized during cell fractionation when the interaction between DMS DH and cytochrome c_2 is disrupted. A similar situation has been observed in sulfite oxidase, where a Mo(V), ferrocytochrome *b* species can be generated by addition of sulfite in the absence of an oxidant of the ferrocytochrome *b* (*44*).

Another distinguishing feature of type I and type III enzymes is that the former has a Mo−OH group while the latter has a Mo═O moiety. In the absence of any X-ray crystal structures for type II enzymes, spectroscopic studies can provide detailed structural information about the metal center. Two distinct EPR signals have been described in nitrate reductase that show a pH-dependent interconversion. The high-pH Mo(V) form is thought to contain a Mo═O group. Protonation of the molybdenum ligand to generate a Mo−OH group produces the low-pH Mo(V) form (*13*). Our results show that in DMS DH the situation is slightly different; the low-pH Mo(V) form is a Mo−aqua species,

and this forms a Mo−OH species as the pH is raised. Interestingly, the maximum specific activity occurs at pH 9.27.

Sequence analysis has shown that the β-subunits of nitrate reductase, selenate reductase, and DMS DH are all related (*1*). In the case of nitrate reductase it is well established that NarH contains two high-potential iron−sulfur clusters, center 1, a $[4Fe\text{-}4S]^{2+,1+}$ cluster, and center 2, a $[3Fe\text{-}4S]^{1+,0}$ cluster, and two low-potential iron−sulfur clusters, centers 3 and 4, both $[4Fe\text{-}4S]^{2+,1+}$ clusters (*8*). Metal ion analysis of DMS DH suggests the enzyme possesses sufficient Fe to form the four iron−sulfur clusters found in NarH (*1*). In this study EPR spectroscopy identified at least two EPR-active species arising from iron−sulfur clusters in DMS DH. One of these is the $[3Fe\text{-}4S]^{1+,0}$ iron−sulfur cluster, a high-potential redox center that, by analogy with NarH, is likely to be involved in electron transfer to the cytochrome (*45*).

There are three possible redox states for [4Fe-4S] clusters, namely, $[4Fe\text{-}4S]^{3+}$, $[4Fe\text{-}4S]^{2+}$, and $[4Fe\text{-}4S]^{1+}$ (*46*, *47*). While the $3^+/2^+$ redox couple ($E^0 \sim 50-500$ mV) is found in high-potential iron−sulfur proteins (HIPIP), the $2^+/1^+$ redox couple ($E^0 \sim -300$ to -700 mV) is usually found in ferredoxins and reductases (*46*, *47*). The $[4Fe\text{-}4S]^{3+}$ clusters are comprised of mixed-valence ($Fe^{2.5+}-Fe^{2.5+}$) and ferric ($Fe^{3+}-Fe^{3+}$) pairs giving rise to an $S = {}^1/_2$ ground state (*30*). A one-electron reduction produces the $[4Fe\text{-}4S]^{2+}$ cluster which can be considered as made up of two $[2Fe\text{-}2S]^{2+}$ dimers in which double exchange operates, producing four equivalent $Fe^{2.5+}$ atoms and a diamagnetic $S = 0$ ground state (*30*). The $[4Fe\text{-}4S]^{+}$ clusters are comprised of mixed-valence ($Fe^{2.5+}-Fe^{2.5+}$) and ferrous ($Fe^{2+}-Fe^{2+}$) pairs, also giving rise to an $S = {}^1/_2$ ground state (*30*).

In the EPR spectrum of the native DMS DH (Figure 2c,d) the resonances associated with the [4Fe-4S] cluster are weak but upon reduction increase in intensity, suggesting the presence of a $[4Fe\text{-}4S]^{1+}$ cluster. Density functional theory has been used to determine the electronic structure of the $[4Fe\text{-}4S]^{3+}$ and $[4Fe\text{-}4S]^{1+}$ clusters and to calculate the principal values and direction cosines of their *g* matrices (*48*). *g* is approximately axially symmetric with g_{av} greater than g_e (2.00232) for the $[4Fe\text{-}4S]^{3+}$ clusters, while for $[4Fe\text{-}4S]^{1+}$ clusters, *g* is rhombic with g_{av} less than g_e [compare sites 1 and 7 for γ-irradiated single crystals of the asymmetric $[Fe_4S_4(SC_6H_4\text{-}o\text{-}OH)_4]^{2+}$ cluster (*49*) listed in Table 3]. g_{av} (1.9216, Table 3) for the [4Fe-4S] cluster in DMS DH is significantly less than g_e, indicating the presence of a $[4Fe\text{-}4S]^{+}$ cluster. However, a comparison of the *g* matrix and its trace (g_{av}) for this cluster with those of other $[4Fe\text{-}4S]^{+}$ cluster containing proteins (apart from the minor conformer in NarH), for example, formate dehydrogenase (FDH) and periplasmic nitrate reductase (NAP) (cf. Table 3), reveals significant differences. These are highlighted by a comparison of Δg ($\Delta g = g_e - g_{av}$) for the $[4Fe\text{-}4S]^{+}$ cluster in DMS DH (0.0817), FDH (0.0483), and NAP (0.0523). In the latter proteins (FDH and NAP) four cysteine residues (C-X_2-C-X_3-C-X_{26}-C) complete the coordination sphere of the iron atoms. The *g* matrix and g_{av} of DMS DH are more similar to $[4Fe\text{-}4S]^{+}$ clusters which have non-sulfur (cysteine) ligating atoms, for example, the citrate, nitroisocitrate, and *trans*-aconitase complexes of the $[4Fe\text{-}4S]^{+}$ cluster in aconitase, site 7 in γ-irradiated single crystals of the asymmetric $[Fe_4S_4(SC_6H_4\text{-}o\text{-}OH)_4]^{2+}$ cluster (cf. Table 3) where coordination of oxygen atoms from the substrate/inhibitor or ligand occurs.

Thus, one possibility is that the $[4Fe\text{-}4S]^{+}$ cluster that we have identified in DMS DH has at least one non-sulfur (cysteine) ligand. However, the presence of a non-sulfur ligand is inconsistent with the sequence data for the $[4Fe\text{-}4S]^{+}$ cluster identified at the beginning of the sequence of the DMS DH β-subunit which shows absolute conservation of the four Cys residues. This cluster is predicted from sequence alignments to be the equivalent of center 1 in NarH. EPR studies of the redox centers in NarH revealed that the $[4Fe\text{-}4S]^{+}$ cluster (center 1) existed in two conformations in different proportions. The minor conformer has a *g* matrix, Δg, and rhombicity parameters (Table 3) very similar to those found for the $[4Fe\text{-}4S]^{+}$ cluster in DMS DH (33). The high anisotropy of the $[4Fe\text{-}4S]^{+}$ cluster in DMS DH may arise from a distortion in the classical cubane arrangement of the $[4Fe\text{-}4S]^{+}$ cluster through coordination of a N or an O atom from a neighboring amino acid such as Ser23 or Lys209. The two conformers in NarH may arise from an equilibrium involving the coordination/dissociation of a fifth ligating atom (N or O) to an Fe atom in the cluster. The minor conformer corresponds to the cluster in which the fifth ligand is coordinated. The absence of a second conformation of the $[4Fe\text{-}4S]^{+}$ cluster in DMS DH suggests that the fifth ligand is more strongly bound. We note that other ferredoxins can also exist in two conformations. EPR studies of the $[4Fe\text{-}4S]^{+}$ cluster in ferredoxin I from *Desulfovibrio africanu*s reveal two rhombic EPR signals (Table 3) which integrate to 1.0 spin/molecule (*50*). Subsequently, X-ray crystallography (*51*) has identified the origin of these two conformations. There is a fifth cysteine residue in which the sulfur atom is within the van der Waals contact of the labile sulfide in the cluster and the cysteic sulfur. The EPR parameters (Table 3) for this cluster are quite different from those for DMS DH, suggesting that a fifth ligand interacts with iron and not the labile sulfide in DMS DH.

Another possibility, albeit remote, is that the $[4Fe\text{-}4S]^{+}$ cluster that we have observed is not bound to DdhB but instead is bound to the α-subunit of DMS DH. The MPT-containing α-subunits of type II enzymes are typified by a cysteine-rich motif (H-X_3-C-X_3-C-X_{34}-C) at the N-terminus (*1*, *52*). This motif is similar to one found at the N-terminus of type I enzymes such as formate dehydrogenase (C-X_2-C-X_3-C-X_{26}-C). In type I enzymes the presence of a [4Fe-4S] cluster at the N-terminus is established. This leads to the possibility that in DMS DH the unusual $[4Fe\text{-}4S]^{+}$ cluster that contains a non-sulfur ligand arises from a motif at the N-terminus of the α-subunit and not from the β-subunit. While this possibility cannot be ruled out, no strong evidence for the presence of such an [Fe-S] cluster has emerged from experiments with nitrate reductase (NarGH) (*7*, *52*). Pulsed EPR or electron−nuclear double resonance experiments would be able to provide more detailed information on this center, and this study will need to be linked to site-directed mutagenesis studies as performed previously for NarGH.

Upon further reduction of DMS DH a complex EPR spectrum containing resonances from at least one or more additional low-potential iron−sulfur clusters is observed (results not shown). The complexity of the spectrum suggests spin−spin interactions between one or more of the redox-active centers in DMS DH. Spin−spin interactions involving

the [4Fe-4S] clusters in NarH have also been suggested (*8*, *53*). As a consequence, given the Fe content of the enzyme and the high similarity between the β-subunits of the two enzymes, it is probable that DdhB coordinates two low-potential iron−sulfur clusters. However, further spectroscopic analysis linked to redox potentiometry is needed to complete the analysis of iron−sulfur clusters in DMS DH.

DMS DH and selenate reductase are distinguished from the respiratory nitrate reductase by a number of important features. First, DMS DH and selenate reductase are both periplasmic enzymes (*2*, *54*) while the NarGH dimer is peripheral membrane protein, facing toward the cytoplasm (*10*), and is anchored to the membrane by the membrane-spanning NarI subunit. The NarI subunit is a quinol-oxidizing diheme (*10*, *31*, *55*). In contrast to DMS DH and selenate reductase which contain *b*-type hemes and are monomeric, they were not too closely related to NarI. Phenotypic analysis of the *ddhC* mutant indicated that this polypeptide was the *b*-type cytochrome in DMS DH, and by analogy the same properties are likely for the SerC subunit of selenate reductase. The presumed role of *b*-type cytochrome in DMS DH is to transfer electrons out of the enzyme to a periplasmic electron acceptor. Our recent characterization of a *cycA* mutant of *R. sulfidophilum* shows that cytochrome c_2 functions as this electron acceptor and has a critical role in mediating electron transfer from DMS DH to the photochemical reaction center (*1*). The midpoint redox potential for the *b*-type cytochrome in DMS DH is quite high, and this value would be consistent with a role for this redox center in electron transfer out of the enzyme. Finally, our MCD spectroscopic study indicates that the axial ligands in the *b*-type heme are provided by histidine and methionine. We have already noted that His81 and Met147 in DMS DH are conserved in selenate reductase. Thus, we conclude that these residues are involved in coordination of the iron in the *b*-type cytochrome found in selenate reductase.

ACKNOWLEDGMENT

We thank Professor Andrew Thomson and Professor David Richardson for use of facilities in the Center for Metalloprotein Spectroscopy and Biology at the University of East Anglia.

SUPPORTING INFORMATION AVAILABLE

Figure S1 showing the X-band (υ = 9.579 GHz) EPR spectrum of DMS dehydrogenase at 120 K and Figure S2 showing the room temperature MCD spectra of oxidized DMS DH. This material is available free of charge via the Internet at http://pubs.acs.org.

REFERENCES

1. McDevitt, C. A., Hugenholtz, P., Hanson, G. R., and McEwan, A. G. (2002) *Mol. Microbiol. 44*, 1575−1587.
2. Hanlon, S. P., Holt, R. A., Moore, G. R., and McEwan, A. G. (1994) *Microbiology 140*, 1953−1958.
3. Hanlon, S. P., Toh, T. H., Solomon, P. S., Holt, R. A., and McEwan, A. G. (1996) *Eur. J. Biochem. 239*, 391−396.
4. Kisker, C., Schindelin, H., and Rees, D. C. (1997) *Annu. Rev. Biochem. 66*, 233−267.
5. McEwan, A. G., Ridge, J. P., McDevitt, C. A., and Hugenholtz, P. (2002) *Geomicrobiol. J. 19*, 3−21.
6. Richardson, D. J. (2001) *Cell. Mol. Life Sci. 58*, 163−164.
7. Blasco, F., Guigliarelli, B., Magalon, A., Asso, M., Giordano, G., and Rothery, R. A. (2001) *Cell. Mol. Life Sci. 58*, 179−193.
8. Guigliarelli, B., Magalon, A., Asso, M., Bertrand, P., Frixon, C., Giordano, G., and Blasco, F. (1996) *Biochemistry 35*, 4828−4836.
9. Boyington, J. C., Gladyshev, V. N., Khangulov, S. V., Stadtman, T. C., and Sun, P. D. (1997) *Science 275*, 1305−1308.
10. Blasco, F., Iobbi, C., Giordano, G., Chippaux, M., and Bonnefoy, V. (1989) *Mol. Gen. Genet. 218*, 249−256.
11. Rothery, R. A., Blasco, F., Magalon, A., and Weiner, J. H. (2001) *J. Mol. Microbiol. Biotechnol. 3*, 273−283.
12. Hille, R. (1997) *J. Biol. Inorg. Chem. 2*, 804−809.
13. Vincent, S. P., and Bray, R. C. (1978) *Biochem. J. 171*, 639−647.
14. Bray, R. C. (1980) *Adv. Enzymol. Relat. Areas Mol. Biol. 51*, 107−165.
15. Bray, R. C. (1988) *Q. Rev. Biophys. 21*, 299−329.
16. Bray, R. C., Vincent, S. P., Lowe, D. J., Clegg, R. A., and Garland, P. B. (1976) *Biochem. J. 155*, 201−203.
17. Penfold, R. J., and Pemberton, J. M. (1992) *Gene 118*, 145−146.
18. Hirsch, P. R., and Beringer, J. E. (1984) *Plasmid 12*, 139−141.
19. Masepohl, B., Klipp, W., and Puhler, A. (1988) *Mol. Gen. Genet. 212*, 27−37.
20. Laemmli, U. (1970) *Nature 227*, 680−685.
21. Thomas, P. A., Ryan, D., and Ledwin, W. (1976) *Anal. Biochem. 75*, 168−176.
22. Griffin, M., Muys, A., Noble, C., Wang, D., Eldershaw, C., Gates, K. E., Burrage, K., and Hanson, G. R. (1999) *Mol. Phys. Rep. 26*, 60−84.
23. Heichel, M., Hofer, P., Kamlowski, A., Griffin, M., Muys, A., Noble, C., Hanson, G. R., Eldershaw, C., Gates, K. E., and Burrage, K. (2000) *Bruker Rep. 149*, 6−9.
24. Pilbrow, J. R., and Hanson, G. R. (1993) *Methods Enzymol. 227*, 330−353.
25. Thomson, A. J., Cheesman, M. R., and George, S. J. (1993) *Methods Enzymol. 226*, 199−232.
26. Dutton, P. L. (1978) *Methods Enzymol. 54*, 411−435.
27. Gutteridge, S., Bray, R. C., Notton, B. A., Fido, R. J., and Hewitt, E. J. (1983) *Biochem. J. 213*, 137−142.
28. Gutteridge, S., Tanner, S. J., and Bray, R. C. (1978) *Biochem. J. 175*, 869−878.
29. George, G. N., Bray, R. C., Morpeth, F. F., and Boxer, D. H. (1985) *Biochem. J. 227*, 925−931.
30. Mouesca, J. M., and Lamotte, B. (1998) *Coord. Chem. Rev. 180*, 1573−1614.
31. Rothery, R. A., Blasco, F., Magalon, A., Asso, M., and Weiner, J. H. (1999) *Biochemistry 38*, 12747−12757.
32. Cammack, R., and Weiner, J. H. (1990) *Biochemistry 29*, 8410−8416.
33. Guigliarelli, B., Asso, M., More, C., Augher, V., Blasco, F., Pommier, J., Giordano, G., and Bertrand, P. (1992) *Eur. J. Biochem. 307*, 63−68.
34. Cheesman, M. R., Greenwood, C., and Thomson, A. J. (1991) *Adv. Inorg. Chem. 36*, 201−255.
35. Gadsby, P. M. A., Hartshorn, R. T., Moura, J. J. G., Sinclair-Day, J. D., Sykes, A. G., and Thomson, A. J. (1989) *Biochim. Biophys. Acta 994*, 37−46.
36. Moore, G. R., Williams, R. J. P., Peterson, J., Thomson, A. J., and Mathews, F. S. (1985) *Biochim. Biophys. Acta 829*, 83−96.
37. Arciero, D. M., Peng, Q., Peterson, J., and Hooper, A. B. (1994) *FEBS Lett. 342*, 217−220.
38. Cheesman, M. R., Kadir, F. H., Al-Basseet, J., Al-Massad, F., Farrar, J., Greenwood, C., Thomson, A. J., and Moore, G. R. (1992) *Biochem. J. 286*, 361−367.
39. McKnight, J., Cheesman, M. R., Thomson, A. J., Miles, J. S., and Munro, A. W. (1993) *Eur. J. Biochem. 213*, 683−687.
40. Wootton, J. C., Nicolson, R. E., Cock, J. M., Walters, D. E., Burke, J. F., Doyle, W. A., and Bray, R. C. (1991) *Biochim. Biophys. Acta 1057*, 157−185.
41. Kisker, C., Schindelin, H., Baas, D., Retey, J., Meckenstock, R. U., and Kroneck, P. M. H. (1998) *FEMS Microbiol. Rev. 22*, 503−521.
42. Bennett, B., Benson, N., McEwan, A. G., and Bray, R. C. (1994) *Eur. J. Biochem. 225*, 321−331.
43. Bennett, B., Berks, B. C., Ferguson, S. J., Thomson, A. J., and Richardson, D. J. (1994) *Eur. J. Biochem. 226*, 789−798.
44. Kipke, C. A., Cusanovich, M. A., Tollin, G., Sunde, R. A., and Enemark, J. H. (1988) *Biochemistry 27*, 2918−2926.
45. Rothery, R. A., Blasco, F., and Weiner, J. H. (2001) *Biochemistry 40*, 5620−5628.

46. Cammack, R. (1992) *Adv. Inorg. Chem. 38*, 281−322.
47. Johnson, M. K. (1994) in *Encyclopedia of Inorganic Chemistry* (King, R. B., Ed.) pp 1896−1915, John Wiley, Chichester, England.
48. Mouesca, J. M., Noodleman, L., Case, D. A., and Lamotte, B. (1995) *Inorg. Chem. 34*, 4347−4359.
49. LePape, L., Lamotte, B., Mouesca, J. M., and Rius, G. (1997) *J. Am. Chem. Soc. 119*, 9757−9770.
50. Hatchikian, E. C., Cammack, R., Patil, D. S., Robinson, A. E., Richards, A. J. M., George, S., and Thomson, A. J. (1984) *Biochim. Biophys. Acta 784*, 40−47.
51. Sery, A., Housset, D., Serre, L., Bonicel, J., Hatchikian, C., Frey, M., and Roth, M. (1994) *Biochemistry 33*, 15408−15417.
52. Magalon, A., Asso, M., Guigliarelli, B., Rothery, R. A., Bertrand, P., Giordano, G., and Blasco, F. (1998) *Biochemistry 37*, 7363−7370.
53. Magalon, A., Rothery, R. A., Giordano, G., Blasco, F., and Weiner, J. H. (1997) *J. Bacteriol. 179*, 5037−5045.
54. Schröder, I., Rech, S., Krafft, T., and Macy, J. M. (1997) *J. Biol. Chem. 272*, 23765−23768.
55. Magalon, A., Lemesle-Meunier, D., Rothery, R. A., Frixon, C., Weiner, J. H., and Blasco, F. (1997) *J. Biol. Chem. 272*, 25652−25658.
56. George, G. N., Turner, N. A., Bray, R. C., Morpeth, F. F., Boxer, D. H., and Cramer, S. P. (1989) *Biochem. J. 259*, 693−700.
57. Rothery, R. A., Trieber, C. A., and Weiner, J. H. (1999) *J. Biol. Chem. 274*, 13002−13009.
58. Costa, C., Teixeira, M., LeGall, J., Moura, J. J. G., and Moura, I. (1997) *J. Biol. Inorg. Chem. 2*, 198−208.
59. Townson, S. M., Hanson, G. R., Upcroft, J. A., and Upcroft, P. (1994) *Eur. J. Biochem. 220*, 439−446.
60. Breton, J., Berks, B. C., Reilly, A., Thomson, A. J., Ferguson, S. J., and Richardson, D. J. (1994) *FEBS Lett. 345*, 76−80.
61. Werst, M. M., Kennedy, M. C., Beinert, H., and Hoffman, B. M. (1990) *Biochemistry 29*, 10526−10532.
62. Beinert, H., Kennedy, M. C., and Stout, C. D. (1996) *Chem. Rev. 96*, 2335−2373.
63. Duderstadt, R. E., Brereton, P. S., Adams, M. W., and Johnson, M. K. (1999) *FEBS Lett. 454*, 21−26.
64. Conover, R. C., Kowal, A. T., Fu, W. G., Park, J. B., Aono, S., Adams, M. W., and Johnson, M. K. (1990) *J. Biol. Chem. 265*, 8533−8541.

BI026221U